Structural Investigation of the Active Site in Bacteriorhodopsin: Geometric Constraints on the Roles of Asp-85 and Asp-212 in the Proton-Pumping Mechanism from Solid State NMR†

J. M. Griffiths,[‡,§] A. E. Bennett,[‡,||] M. Engelhard,[⊥] F. Siebert,[#] J. Raap,[▽] J. Lugtenburg,[▽] J. Herzfeld,*[,○] and R. G. Griffin*[,†]

Department of Chemistry and MIT/Harvard Center for Magnetic Resonance, Francis Bitter Magnet Laboratory, Massachusetts Institute of Technology, Cambridge, Massachusetts 02139, Genzyme Corporation, 500 Soldiers Field Road, Allston, Massachusetts 02134, Max-Planck-Institut für Molekulare Physiologie, Otto-Hahn-Strasse 11, 44227 Dortmund, Germany, Institut für Biophysik and Strahlenbiologie der Universität, Albertstrasse 23, D-78 Freiberg, Germany, Department of Chemistry, Rijksuniversiteit te Leiden, NL-2300 R A, Leiden, The Netherlands, and Department of Chemistry and Keck Institute for Cellular Visualization, Brandeis University, Waltham, Massachusetts 02454

Received May 14, 1999; Revised Manuscript Received September 21, 1999

ABSTRACT: Constraints on the proximity of the carboxyl carbons of the Asp-85 and Asp-212 side chains to the 14-carbon of the retinal chromophore have been established for the bR_{555}, bR_{568}, and M_{412} states of bacteriorhodopsin (bR) using solid-state NMR spectroscopy. These distances were examined via $^{13}C-^{13}C$ magnetization exchange, which was observed in two-dimensional RF-driven recoupling (RFDR) and spin diffusion experiments. A comparison of relative RFDR cross-peak intensities with simulations of the NMR experiments yields distance measurements of 4.4 ± 0.6 and 4.8 ± 1.0 Å for the [4-^{13}C]Asp-212 to [14-^{13}C]retinal distances in bR_{568} and M_{412}, respectively. The spin diffusion data are consistent with these results and indicate that the Asp-212 to 14-C-retinal distance increases by 16 ± 10% upon conversion to the M-state. The absence of cross-peaks from [14-^{13}C]retinal to [4-^{13}C]Asp-85 in all states and between any [4-^{13}C]Asp residue and [14-^{13}C]retinal in bR_{555} indicates that these distances exceed 6.0 Å. For bR_{568}, the NMR distance constraints are in agreement with the results from recent diffraction studies on intact membranes, while for the M state the NMR results agree with theoretical simulations employing two bound waters in the region of the Asp-85 and Asp-212 residues. The structural information provided by NMR should prove useful for refining the current understanding of the role of aspartic acid residues in the proton-pumping mechanism of bR.

Absorption of light by the retinal group in the 26 kDa integral membrane protein bacteriorhodopsin (bR)[1] initiates a photocycle which transfers protons from the cytoplasm to the extracellular surface (*1*−*3*). This light-driven transport process provides a store of energy for the halophilic archae, *Halobacterium salinarium*. The 248 amino acid polypeptide chain is folded into a bundle of seven transmembrane α-helices (*4*). A retinal chromophore, bound to the side chain of Lys-216 through a Schiff base linkage, resides in the proton transport channel enclosed by the helices. Mechanistic models of proton transport have been proposed based on molecular dynamics simulations (*5*−*9*) and experimental data from many biophysical techniques (*1*). However, complete elucidation of the translocation mechanism requires precise knowledge of the structure of the active site in both the resting state of bR and its photointermediates.

The dark-adapted state of bR comprises a 60:40 mixture of two species: bR_{555} and bR_{568}, with the retinal in 6-s-trans, 13-cis, 15-syn and 6-s-trans, 13-trans, 15-anti conformations, respectively. Irradiation of the dark-adapted mixture with white light converts the bR_{555} to bR_{568}, which is the starting point of the proton pumping cycle. Defining characteristics of the photocycle intermediates, including K_{590}, L_{550}, M_{412}, N_{520}, and O_{640}, include changes in the conformation of the retinal and changes in the protonation states of the Schiff base and ionizable amino acid residues. A critical role has been postulated for the relatively long-lived M_{412} intermediate, since it is the sole photointermediate with a deprotonated Schiff base. It is generally expected that the early M state, which has just released proton to the

† This research was supported by NIH Grants GM-23289, GM-36810, and RR-00995. J.M.G. acknowledges the support of a postdoctoral fellowship from the American Cancer Society and A.B. a predoctoral fellowship from the National Science Foundation.

* To whom correspondence should be addressed. (R.G.G.) E-mail: rgg@mit.edu. (J.H.) E-mail: herzfeld@brandeis.edu.

‡ Massachusetts Institute of Technology.

§ Genzyme Corporation.

|| Present address: Department of Biological Chemistry and Molecular Pharmacology, Harvard Medical School, Boston, MA 02115.

⊥ Max-Planck-Institut für Molekulare Physiologie.

Institut für Biophysik and Strahlenbiologie der Universität.

▽ Rijksuniversiteit te Leiden.

○ Brandeis University.

[1] Abbreviations: bR, bacteriorhodopsin; CPMAS, cross polarization/magic angle spinning; CSA, chemical shift anisotropy; FTIR, Fourier transform infrared spectroscopy; MAS, magic angle spinning; NMR, nuclear magnetic resonance; RF, radio frequency; RFDR, radio frequency driven recoupling; UV−vis, ultraviolet−visible.

10.1021/bi991106d CCC: $19.00
Published on Web 12/17/1999

extracellular side of the membrane, must be different from the late M state which is poised to reprotonate from the intracellular side of the membrane.

Much effort has been focused on the role of ionizable residues as acceptors and donors of protons and their association with water molecules in the proton channel (*11*). Studies of bR mutants have suggested that ionizable aspartate residues lining the channel, including Asp-85, Asp-96, and Asp-212, are important for proton transport (*2*). In particular, while Asp-96 is important in translocating protons from the intracellular surface, Asp-85 and Asp-212 play key roles in shifting protons from the Schiff base to the extracellular surface after light absorption (*12*). Further, attention has focused on the roles of Arg-82, Glu-204, and Glu-194 in completing transfer from the initial proton acceptor, Asp-85, to the extracellular face (*10*, *11*, *13*, *14*). Recent electron cryomicroscopy (*13*, *14*) and X-ray diffraction (*11*, *15*) structures of bR have begun to provide details on hydrogen bonding among residues in the resting state of bR and on the likely role of ordered water molecules in the photocycle. FTIR and NMR spectra indicate that Asp-85 is unprotonated in bR_{568}, K_{590}, and L_{550}, but protonated in M_{412}, while Asp-212 remains deprotonated throughout the photocycle (*1*, *16*). The proton donor to the Schiff base in the second half of the photocycle, Asp-96, is positioned between the retinal and the cytoplasm, approximately 10−12 Å from the Schiff base. In addition to the aspartic acids, the residues Tyr-57, Arg-82, Trp-86, and Tyr-185 contribute to charge-transfer stabilization in the vicinity of the Schiff base (*7*, *11*).

The two solid-state NMR techniques employed here, RFDR (*17*, *18*) and spin diffusion (*19*−*22*), are intended to measure the strength of $^{13}C-^{13}C$ dipolar couplings in magic angle spinning (MAS) experiments by examining polarization exchange. The rate of polarization exchange is reflected in the evolution of cross-peak intensities in two-dimensional (2D) NMR experiments. Both 2D techniques are able to detect internuclear $^{13}C-^{13}C$ distances in the range 4−6 Å and have been successfully utilized to measure the 4.56 Å distance between two ^{13}C nuclei in the model peptide glycylglycine (*18*) and to determine the retinal conformations in dark-adapted bacteriorhodopsin (*23*). The experiments reported here are focused on internuclear distances between a ^{13}C-label at the 14-C position on the retinal chromophore and ^{13}C-labels in the carboxyl groups of the aspartic acid side chains.

RF-driven dipolar recoupling (RFDR) is a longitudinal exchange experiment that utilizes a series of rotor-synchronized π pulses to reintroduce homonuclear dipole−dipole couplings that are otherwise attenuated by MAS (*17*, *18*). Experimental cross-peak intensities reflecting magnetization exchange are compared to simulations of the NMR experiment to extract distance information. In contrast polarization exchange experiments based on spin diffusion, which occurs among ^{13}C nuclei in the absence of proton decoupling, is a second approach to examining the strength of dipole−dipole couplings (*19*, *20*). This effect relies on the broadening of the ^{13}C line widths, via heteronuclear dipolar interactions with the protons, to mediate transfer of magnetization among ^{13}C sites. A complete description of spin diffusion is theoretically complex because it relies on the dynamics of the entire bath of many strongly coupled protons in the sample (*20*). However, it has been shown that spin diffusion is an exponential process in the relatively slow spinning regime employed here, and that the rate is proportional to $1/r_{12}^6$, where r_{12} is the distance between the ^{13}C atoms (*21*, *22*).

MATERIALS AND METHODS

Sample Preparation. Bacteriorhodopsin was biosynthetically labeled by introducing [4-^{13}C]aspartic acid into a defined growth medium (*24*, *25*), resulting in the incorporation of the ^{13}C label into the Asp and Asn residues. The incorporation level was determined to be ∼36% by comparison of the intensities of the FTIR bands corresponding to the Asp-85−$^{12}COOH$ and −$^{13}COOH$ stretching frequencies. In addition, ^{13}C isotope was transferred to the 11-carbons of the Trp residues and, to a much lesser extent, the C_0 of the glutamate and glutamine residues. [14-^{13}C]retinal, enriched to 99%, was incorporated by first bleaching bR with hydroxylamine, followed by regeneration with the isotopically labeled retinal as previously described (*28*). The [4-^{13}C]-Asp, [14-^{13}C]retinal bR sample was dispersed in deionized water and repeatedly washed and centrifuged. The extent of the regeneration was 90%, as monitored by UV−vis absorption spectroscopy. Prior to use in experiments on the M_{412} state, the sample was dispersed and washed in 0.3 M guanidine hydrochloride adjusted to pH 10 (*26*). In preparation for MAS, the 80 mg centrifuge pellet was packed into a 5 mm silicon nitride rotor for spinning experiments with spinning frequencies of >5 kHz or into a translucent 7 mm sapphire rotor for rotation at <5 kHz (both obtained from Doty Scientific, Inc.). The translucent rotor was necessary for in situ irradiation to generate the light-adapted and M_{412} photocycle intermediates.

NMR Experimental Procedures. NMR spectra were recorded at 79.9 MHz for ^{13}C, using custom designed variable temperature, double resonance MAS probes with light pipes. The spinning frequency was monitored using a thin fiber optic cable positioned within 2 mm of the bottom end-cap of the sample rotor. The RFDR experiment, shown in Figure 1a, is initiated by cross polarization followed by a chemical shift evolution period, t_1. A pair of $\pi/2$ pulses flanking the longitudinal mixing period τ_{mix} prepares the spin polarizations for exchange and returns them to the transverse plane for further chemical shift evolution during t_2. Rotor synchronized π pulses (one per rotor period) were applied during the mixing period to induce exchange via homonuclear dipole−dipole couplings which are otherwise eliminated by MAS alone. The π pulses were alternated according to the *XY*-16 scheme to compensate for resonance offsets and other pulse errors (*27*). A large mismatch between the ratios of the ^{13}C and ^1H fields, i.e., $\nu_{RF}(^1H)/\nu_{RF}(^{13}C) \geq 2.5$, was maintained with maximum available proton decoupling in order to minimize dephasing of the ^{13}C magnetization from insufficient proton decoupling (*18*). Before performing the 2D dipolar experiments, spin−echo trains were applied to both the transverse and longitudinal magnetization to estimate the time scales for their decay during the pulse cycle.

The two-dimensional spin diffusion exchange experiment, illustrated in Figure 1b, was performed similarly, except that the mixing period consists of a lengthy (>1 s) period of free exchange in the absence of proton decoupling. In this case, strong $^1H-^{13}C$ dipolar interactions promote rapid dephasing

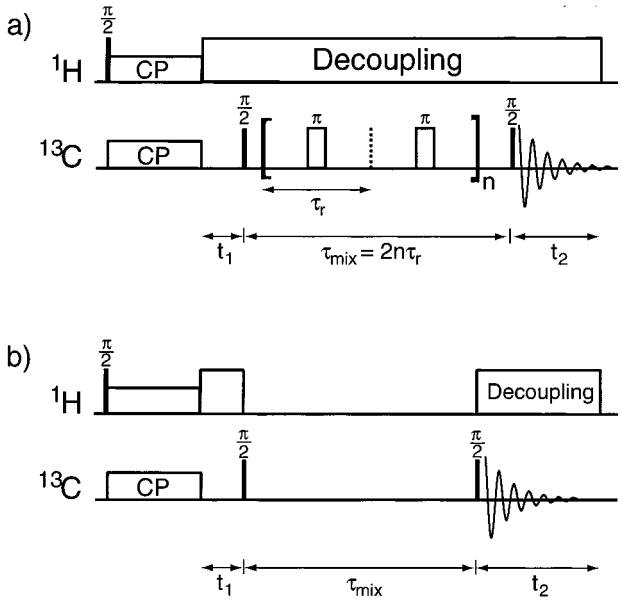

FIGURE 1: (a) The 2D RFDR pulse sequence uses cross polarization to generate rare spin magnetization followed by a t_1 evolution period. A nonselective $\pi/2$ pulse then creates longitudinal polarizations for spin exchange. Rotor-synchronized π pulses are applied once per rotor period during the mixing period τ_{mix}. A second nonselective $\pi/2$ pulse generates observable magnetization which is recorded in t_2. (b) The 2D spin diffusion pulse sequence is identical except that the mixing period consists of a delay during which proton decoupling is inactivated.

of all ^{13}C coherences of transverse character, effectively broadening their line shapes to overcome frequency differences and thereby facilitating slow magnetization exchange among ^{13}C spins (*19*, *21*). This mechanism remains effective even with sample spinning and is also fairly independent of the spinning frequency under conditions where the ^{1}H−^{1}H interactions greatly exceed the spinning rate, as is the case here (*22*). For spin pairs with at least one protonated ^{13}C, however, mixing periods of >1 s are required to observe significant exchange in pairs which are separated by 4−6 Å.

Typical pulse lengths were 3.5 μs for the ^{1}H $\pi/2$ and 5.0 μs for the ^{13}C $\pi/2$ pulses, respectively. During the mixing periods of RFDR experiments performed at 6.2 kHz, where the ^{1}H decoupling power was 95 kHz, the ^{13}C RF power was reduced to 35 kHz (i.e., a 14.3 μs π pulse). This reduction minimized the signal losses attributable to insufficient proton decoupling during the simultaneous application of ^{13}C and ^{1}H RF fields. In the M RFDR experiment, which was performed at 4.805 kHz spinning, the ^{13}C power was reduced to 28 kHz to avoid depolarization, since the ^{1}H decoupling field was 71 kHz.

All bR photocycle intermediates were preserved in the dark by cooling the sample to −90 ± 10 °C with N_2 bearing and drive gases for MAS. Light-adapted bR was prepared by warming dark-adapted bR to 0 ± 5 °C and illuminating the sample with incandescent light for 10 h (*26*). A fiber optic cable, inserted into the probe, was positioned close to the rotor endcap for in situ irradiation of the bR sample (*28*). The M_{412} state was formed from the light-adapted state (dispersed in 0.3 M guanidine hydrochloride at pH 10) by holding the sample temperature at −30 ± 3 °C for 3 h while illuminating with filtered light (>540 nm) (*26*, *29*). In a similar procedure performed outside of the NMR probe, the color of the protein sample changed from purple, which is characteristic of the light and dark-adapted states, to the yellow color that is characteristic of M_{412}. Following in-situ preparation of M in the magnet, the ^{13}C chemical shifts of the [14-^{13}C]retinal resonance converted to the characteristic doublet at 124.0 and 125.7 ppm of the early M state, M_o (*26*, *30*).

The spinning frequency ($\omega_r/2\pi$) stability was maintained to ±2 Hz in RFDR experiments, but only to ±10 Hz in spin diffusion experiments, where precise rotor synchronization is not critical to the dynamics of spin exchange. In general, the weaker cross-peaks and broader retinal line shape in the M state necessitated the acquisition of more scans. In all cases, the transmitter frequency, as well as the spectral window in the t_1 domain, were carefully adjusted in order to ensure that possible aspartate-retinal cross-peaks did not fall in the region of spinning sidebands. The window in t_1 was also set in each case so that sidebands aliased into the 2D spectrum from beyond the narrow t_1 window occurred in the same region as existing sideband intensity. Complete phase cycling to obtain pure absorption phase spectra in the 2D plane was achieved via separate acquisition and recombination of the real and imaginary spectra from the first frequency domain. To minimize effects from small fluctuations in the cross polarization intensity, the 2D spectra were assembled by addition of separate two-dimensional data sets acquired with the complete basic phase cycle of 128 free induction decays for each t_1 slice. Addition of all of the 2D sets was employed in the final processing.

Signal losses corresponding to a given RF power level were measured for all relevant spectral lines in the RFDR experiments, i.e., decay of longitudinal magnetization during the π pulse echo sequence. In the dark-adapted RFDR experiment, <40% of the retinal signal decayed during a 30 ms mixing pulse sequence. For the M_{412} RFDR spectrum, which was recorded with the smaller proton field strength of 71 kHz, <60% of the retinal signal was lost within 30 ms. Such losses are typical in RFDR experiments performed with ^{1}H decoupling fields <100 kHz (*18*).

Quantitative Interpretation of RFDR Cross Peaks. The cross-peaks observed in the labeled bR sample provide direct evidence of proximity within approximately 6 Å between the 14-carbon in the retinal chromophore and the 4-carbon in the Asp-212 side chain. Conversely, the absence of cross-peaks indicates greater separations involving all other aspartic acid residues, including the proton acceptor Asp-85. For separations of <5 Å, we have been able to quantify the cross-peak intensities and obtain approximate internuclear distances by comparison with exact simulations of the RFDR experiments (*18*). Retinal conformations in bR_{555} and bR_{568} have already been determined using this approach and agreed with a previous determination (*23*). Simulations also establish the maximum distance (i.e., the weakest dipole−dipole coupling) which leads to observable cross-peaks under these experimental conditions.

The basis of dipolar exchange in RFDR is interference between the action of the π pulse train and MAS. This results in an effective average spin Hamiltonian involving a pair of spins 1 and 2:

$$\bar{H}_D^{eff} = -\frac{1}{2}\bar{d}_{12}[I_{+1}I_{-2} + I_{-1}I_{+2}] \qquad (1)$$

where in the simple case of neglect of chemical shift anisotropy the effective coupling constant is given by the approximation (*17*)

$$\bar{d}_{12} = \frac{2}{\pi} \sum_{m=1,2} \left\{ \frac{\Delta\delta/\nu_r}{m^2 - (\Delta\delta/\nu_r)^2} \right\} (-1)^{m-1} \hat{d}_{12}[m](\theta) \cos(m\phi) \sin\left\{ \pi \frac{\Delta\delta}{\nu_r} \right\} \quad (2)$$

In eq 2, $\Delta\delta$ represents the chemical shift difference between the two spins, ν_r is the rotor frequency, and $\hat{d}_{12}[m](\theta)$ is the mth Fourier component of the dipolar coupling during sample spinning. The angles (θ,ϕ) relate the internuclear vector to the rotor-fixed reference frame. The parameters $\hat{d}_{12}[m]$ and, therefore, $\bar{d}_{12}$ are directly proportional to $1/r_{12}^3$ and are accordingly very sensitive to the internuclear separation. Under longitudinal transfer conditions, polarization exchange pursues the following trajectory in RFDR experiments:

$$\rho(\tau) = I_{z1} \cos^2\{2\pi\bar{d}_{12}\tau/2\} + I_{z2} \sin^2\{2\pi\bar{d}_{12}\tau/2\} + [I_{y1}I_{x2} - I_{x1}I_{y2}] \sin\{2\pi\bar{d}_{12}\tau\} \quad (3)$$

Equation 2 implies that exchange is most efficient when the chemical shift difference between the spins is similar to the rotor frequency, which is roughly obeyed in the experiments presented here. Likewise, eq 2 implies very slow exchange among ^{13}C-Asp resonances, which have very similar chemical shifts (i.e., $\Delta\delta \approx 0$, for which $\bar{d}_{12} \approx 0$).

Although these expressions are analytical approximations, in practice, quantitative determinations of internuclear distances are made using exact numerical simulations. In particular, the cross-peak corresponding to exchange from the [14-^{13}C]retinal polarization to the [4-^{13}C]Asp-212 resonance is most useful for quantification of the RFDR data because an estimate of the diagonal intensity can be obtained for the fairly isolated retinal peak. Due to spectral crowding among the Asp residues, it is difficult to obtain estimates of diagonal peak intensities in that region. Further, because of differing rates of ^{13}C magnetization decay and unequal cross polarization intensities between the [14-^{13}C]retinal and [4-^{13}C]Asp-212 resonances, the two off-diagonal exchange peaks are not expected to have the same intensities. For all of these reasons, only exchange from retinal to Asp-212 exchange process can be treated quantitatively here. The 36% ^{13}C-labeling efficiency in Asp-212 and estimates of the background intensity in the region of the retinal peak (<30% at 4.8 kHz and <10% at 6.2 kHz) were also considered in the analysis. The range of uncertainty in these parameters and the estimated error in the measured intensities (as derived from the overall signal-to-noise ratio of approximately 7:1 for cross-peaks integrated over two dimensions in all of the RFDR experiments) are included as experimental uncertainties.

Signal loss parameters for the longitudinal polarizations of the retinal peak were also included explicitly in the numerical simulations of RFDR exchange. Calculations indicate, however, that the ratio of the cross-peak to the diagonal intensity, which is measured most directly in these experiments, and the associated internuclear distance are fairly insensitive to the rate of loss in retinal polarization during the pulse cycle. Distributions in the decay of the zero quantum coherences associated with the spin pair have likewise been considered in the estimation of the internuclear distances in the bR_{568} and M_{412} states. These were obtained from estimates of the transverse dephasing induced by insufficient proton decoupling under the experimental conditions employed here, using a computational model from ref *18*. The minimum effective zero quantum dephasing time constants, which are 27.4 ms in bR_{568}, but possibly as short as 8.7 ms in the M_{412} RFDR experiment, are compatible with previous experience with model peptide compounds. This effect was almost negligible for bR_{568}, where a 95 kHz proton decoupling field was applied but contributed significant uncertainty to the final estimate of the internuclear distance in M. The analysis also considered the uncertainty introduced by the unknown relative orientations of the internuclear vector and the chemical shift anisotropy (CSA) tensors of the [14-^{13}C]retinal and [4-^{13}C]Asp-212 peaks. The orientation dependence of these interactions contributed only about 4% uncertainty in the M state data taken at $\omega_r/2\pi = 4.805$ kHz, but shifted the estimate of the distance up by 5% in the bR_{568} data acquired at 6.2 kHz (with an uncertainty of ±6%). At 4.805 kHz spinning frequency, the CSA orientations are less important than at 6.2 kHz because the slower frequency is closer to rotational resonance, where the influence of CSA on the exchange rate is reduced. The principal values of the CSA tensors are already known for both [4-^{13}C]Asp-212 (*31*) and [14-^{13}C]retinal (*24*).

Theoretical Analysis of Spin Diffusion Spectra. The interpretation of spin diffusion spectra has the advantage that no multiple pulse sequence is employed to generate dipole−dipole exchange. Instead, the proton decoupling is turned off during the mixing period to facilitate ^{13}C−^{13}C exchange via the line-broadening mechanism of ^{1}H−^{13}C couplings. The primary disadvantage of this approach is that the dynamics of spin diffusion are difficult to describe quantitatively. Nevertheless, in a typical organic solid, available theories predict that spin diffusion is an exponential process for any given crystallite under relatively slow spinning conditions (*22*). The rate, in turn, depends on the internuclear separation r_{12} in the following simple way:

$$\Gamma = \frac{1}{r_{12}^6} f(\tau_c) \quad (4)$$

where $f(\tau_c)$ is some function of the ^{1}H−^{13}C couplings and the "correlation time" τ_c of proton reservoir (*19*−*21*). In general, precise calculation of $f(\tau_c)$ would require the solution of a complicated many-body problem involving many protons. However, it is known that for spin pairs involving at least one protonated carbon, the rate is only weakly dependent on the spinning speed (*20*, *22*). A simple example of spin diffusion is provided by the dipeptide 1,4-^{13}C-glycylglycine hydrochloride, where at $\omega_r/2\pi = 9$ kHz, the rate fits a single-exponential rather well. A measured rate of $\Gamma = 0.35 \pm 0.08$ kHz was obtained experimentally for an internuclear separation of 4.56 Å between the CH_2 and CO_2^- (*32*). Note that the glycylglycine data were acquired at $\omega_r/2\pi = 9$ kHz and the proton correlation times among different organic samples can vary from about 10−40 μs (*33*). Nevertheless, it is interesting to compare the present measurements with those from this well-characterized model

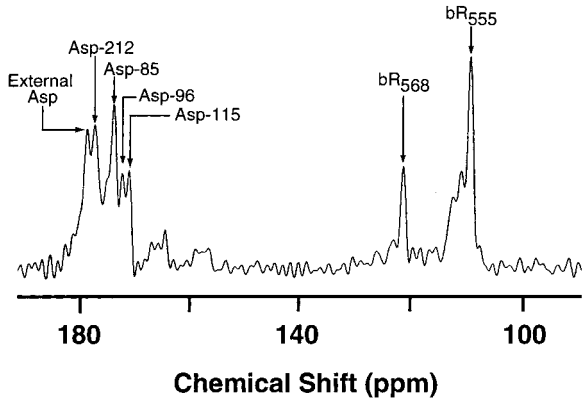

FIGURE 2: One-dimensional CPMAS difference spectrum between [4-^{13}C]Asp, [14-^{13}C]retinal bR in the dark-adapted state and the comparable natural abundance spectrum.

compound, which possesses a comparably weak dipolar coupling (*18*).

RESULTS

MAS Spectra. Figure 2 illustrates the CPMAS spectrum of [4-^{13}C]Asp, [14-^{13}C]retinal bR with subtraction of the spectrum of the natural abundance sample taken under similar conditions. The difference spectrum yields several resolved resonances for aspartate residues that are important in proton transfer, especially the Asp-85, Asp-212, and Asp-96 residues, which have been assigned by Engelhard and co-workers (*16*, *25*). Analysis of the carboxyl side-chain chemical shifts revealed that Asp-212 is unprotonated in both the light-adapted ground state and in the M intermediate, while Asp-85 passes from the unprotonated to the protonated state upon formation of M_{412} in the D96N mutant of bR (*16*). This observation is consistent with FTIR evidence for Asp-85 as the proton acceptor. Figure 3 compares CPMAS spectra of [4-^{13}C]Asp, [14-^{13}C]retinal bR in the light-adapted (top) and M_{412} (middle) states. The difference spectrum (bottom) illustrates the chemical shift differences between these states and implies a high degree of conversion to the deprotonated Schiff base photointermediate M_{412}. In this experiment, the M state was generated by cryogenic trapping of wild-type bR as described above, and the chemical shift changes in Asp-85 and Asp-212 are in good agreement with those determined by Engelhard and co-workers for the D96N mutant (*25*).

The chemical shifts for the labeled retinal peak and the aspartate residues that are relevant here are shown in Table 1. Lines from the carboxyl side-chain carbons appear in the range 170−178 ppm. The four interior aspartate residues, Asp-85, Asp-96, Asp-115, and Asp-212, are relatively sharp and resolved owing to the ordered environment prevailing in the binding pocket (*24*). The [14-^{13}C]retinal resonance line is at 122.0 ppm in bR_{568} and 110.0 ppm in bR_{555} (*26*), the latter peak overlapping with the [11-^{13}C]Trp resonances in the range 110−114 ppm. Upon formation of M_{412}, the [14-^{13}C]retinal signal shifts from 122.0 to a split peak at 124.0 and 125.7 ppm, while Asp-85 shifts from 174.0 to 169.0 ppm and Asp-212 shifts from 176.0 to 177.6 ppm. In both the ground and M states, cross-peaks among the 14-C-retinal, Asp-85, and Asp-212 can be resolved in two-dimensional spectra because of the resolved differences in ^{13}C chemical shifts.

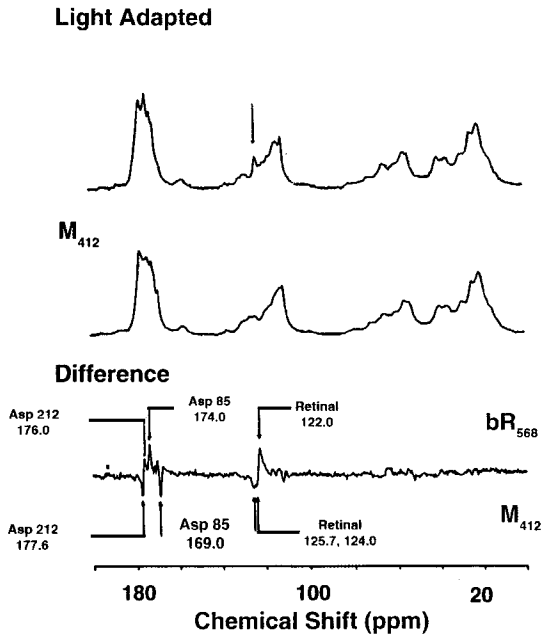

FIGURE 3: CPMAS Spectra of [4-^{13}C]Asp, [14-^{13}C]retinal bR in the light-adapted state (top) and M_{412} state (middle). The difference spectrum (bottom) is shown to emphasize the changes in chemical shifts observed for [14-^{13}C]retinal, [4-^{13}C]Asp-85, and [4-^{13}C]Asp-212 upon conversion from bR_{568} to M_{412}. Other Asp peaks exhibit no discernible shifts. The light-adapted and M_{412} states were generated in situ as described in the text. Each component consists of approximately 8000 scans acquired at $\omega_r/2\pi = 4.300$ kHz.

Table 1: Isotropic ^{13}C Chemical Shifts (in parts per million) in the BR Photointermediates BR_{555}, BR_{568} and M_{412}[a]

^{13}C position	bR_{555}	bR_{568}	M_{412}
4-Asp-212	176.0[b]	176.0	177.6
4-Asp-85	172.9[b]	174.0	169.0
14-C-retinal	110.0	122.0	124.0, 125.7

[a] Shifts are reported relative to TMS. Absolute values for all of the shifts in the table agree within <0.8 ppm with the previous measurements of refs *16*, *24*, *26*, and *30*. [b]Values given by Metz et al. in ref *24*, who reported a shift in Asp-85 only between bR_{555} and bR_{568}.

Two-Dimensional RFDR Spectra. Figure 4 shows the 2D RFDR spectrum of dark-adapted bR recorded with a mixing time of $\tau_{mix} = 31$ ms at 6.200 kHz spinning frequency. A pair of cross-peaks, corresponding to the transfer of polarizations between [14-^{13}C]retinal and the [4-^{13}C]Asp-212 resonance in bR_{568}, is readily observable, while no other cross-peaks among labeled ^{13}C sites are detectable. Cross-peak intensities were determined relative to the diagonal [14-^{13}C]-retinal peak for mixing times of both $\tau_{mix} = 21$ ms and $\tau_{mix} = 31$ ms. No cross-peaks were detected between the [14-^{13}C]retinal in bR_{555} and any aspartic acid residues. Spectra recorded at $\tau_{mix} = 0$ ms yielded no cross-peaks, confirming that their origin is due to dipolar exchange.

Figure 5 shows a similar RFDR spectrum of the M_{412} state taken at 4.805 kHz spinning speed. The cross-peak between the [4-^{13}C]Asp-212 and [4-^{13}C]retinal is again evident, and its position is consistent with the changes in ^{13}C chemical shifts which accompany conversion to the M state.

With consideration of the experimental uncertainties discussed above, the estimated distance between the [14-^{13}C]retinal and the [4-^{13}C]Asp-212 is 4.4 ± 0.6 Å in bR_{568} and 4.8 ± 1.0 Å in M_{412}, based on calculations of the ratio

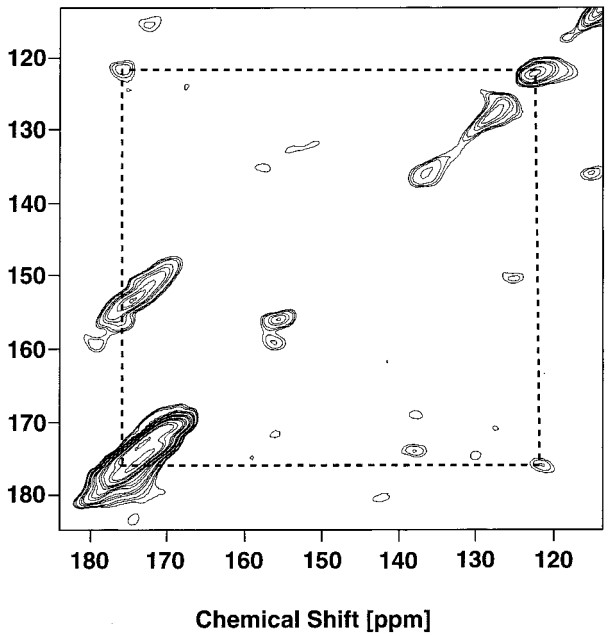

FIGURE 4: 2D RFDR spectrum of dark-adapted [4-^{13}C]Asp, [4-^{13}C]-retinal bR recorded with a mixing time of 31 ms at 6.2 kHz spinning speed, utilizing 24 t_1 slices with 1200 scans/slice. The observed pair of dipolar cross-peaks corresponds to exchange between [4-^{13}C]-Asp-212 and [4-^{13}C]retinal in bR_{568}. No other dipolar cross-peaks are seen. The cross-peaks were positioned between the sideband manifolds that appear at multiples of the spinning frequency. The latter do not correspond to dipolar exchange and must be positioned away from the regions of expected cross-peaks through proper selection of the spectra windows, spinning speed, and reference frequency.

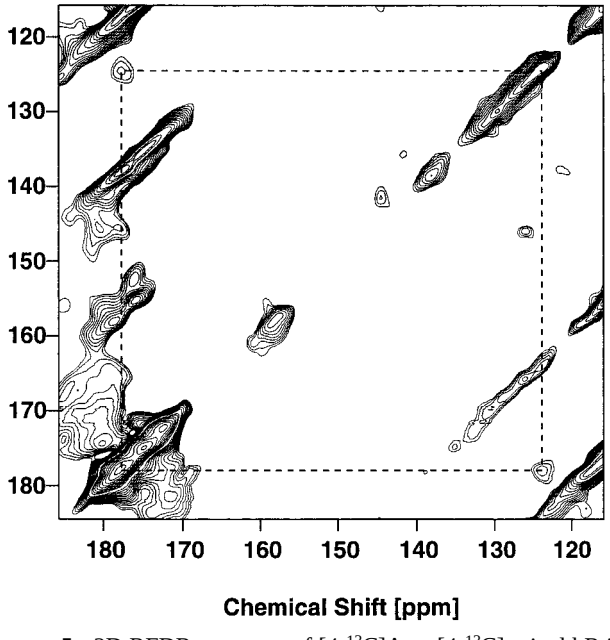

FIGURE 5: 2D RFDR spectrum of [4-^{13}C]Asp, [4-^{13}C]retinal bR in the M_{412} state recorded with a mixing time of 30 ms at $\omega_r/2\pi = 4.805 \pm 0.002$ kHz and utilized 3688 scans for each of 24 t_1 values. The observed pair of dipolar cross-peaks again corresponds to exchange between [4-^{13}C]Asp-212 and [4-^{13}C]retinal in bR_{568}, and as before no other dipolar cross-peaks are seen. The M state was generated in situ as described in the text.

of the cross-peak to diagonal intensities in the RFDR experiments, as compared to experimental values. These were 0.14 ± 0.03 at 21 ms and 0.23 ± 0.05 at 31 ms for the light-adapted state at 6.200 kHz and 0.124 ± 0.025 at 30 ms for

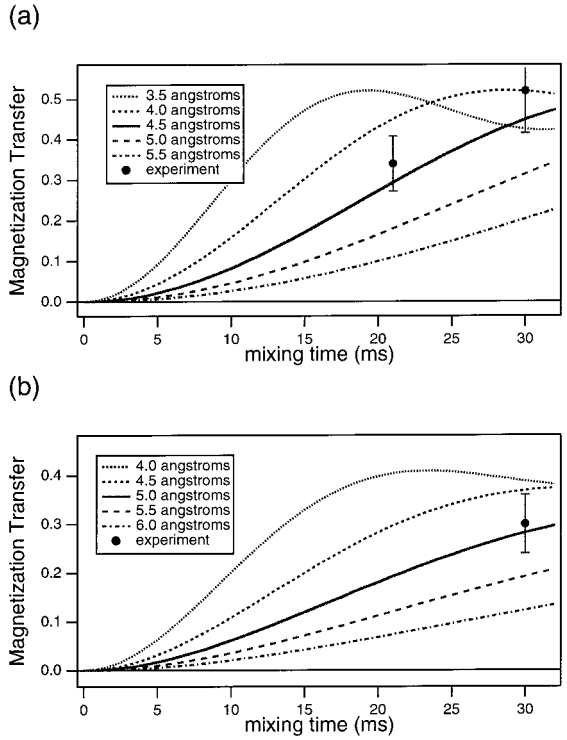

FIGURE 6: (a) Simulations of RFDR exchange between [4-^{13}C]-Asp-212 and [14-^{13}C]retinal for various internuclear distances compared with experimental data for the light-adapted state at $\omega_r/2\pi = 6.2$ kHz. (b) Simulations for the same spin pair in the M_{412} state at 4.805 kHz spinning frequency. Chemical shift anisotropies are neglected, but a dephasing time of 17.4 ms and finite pulses are included. For simplicity, the experimental cross-peaks were derived from the measured ratio of off-diagonal to diagonal intensity under the assumption that the two peaks decay at the same rates during the pulse cycle. However, this assumption was not applied in the derivation of experimental distances.

the M state at 4.805 kHz. Figure 6 illustrates the sensitivity of the cross-peak data to internuclear separation by comparing finite pulse simulations with experimental cross-peak intensities. For simplicity the simulations shown in Figure 6 neglect the effects of signal losses, zero quantum dephasing, and chemical shift anisotropy, although these were included in final estimates of the internuclear distances.

The analysis of the dark-adapted spectra assumed that dipolar exchange between the [4-^{13}C]Asp and [14-^{13}C]retinal peaks in bR_{555} and bR_{568} are not correlated because these two molecules are sufficiently large to constitute two separate and dilute spin systems. The possibility exists for multiple exchange among two or more aspartate sites, but such processes are unlikely both because of the dilute population of ^{13}C-Asp in the sample and the inherently slow exchange among degenerate spins (i.e., $\Delta\delta \approx 0$) in RFDR experiments.

Spin Diffusion Experiments. Figure 7 shows the two-dimensional spin diffusion spectra of light-adapted bR and the M_{412} state under identical conditions with a total mixing period of 2000 ms. Relatively long mixing times are necessary in these experiments in order to achieve significant dipolar exchange for $^{13}C-^{13}C$ distances on the order of 5 Å for spin pairs in which at least one carbon is protonated. Negligible losses in the longitudinal magnetization were fortunately encountered here because the T_1 values of the ^{13}C-Asp and [14-^{13}C]retinal resonances were found to greatly exceed 10 s at low temperature. A cross-peak pair is evident

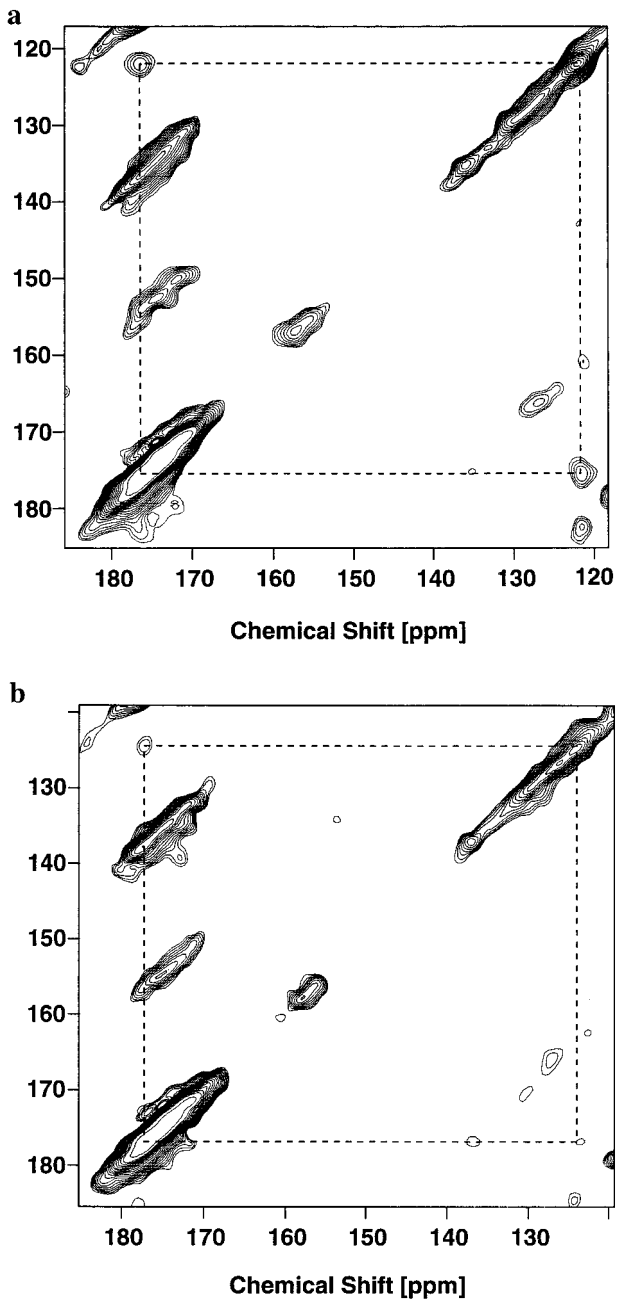

FIGURE 7: (a) 2D spin diffusion spectrum of light-adapted [4-^{13}C]-Asp, [14-^{13}C]retinal bR recorded with a 2000 ms mixing period, $\omega_r/2\pi = 4.805 \pm 0.010$ kHz, and 24 t_1 slices. (b) 2D spin diffusion spectrum of M_{412} for the sample under identical conditions. In both cases, dipolar cross-peaks were once again seen only between Asp-212 and the 14-C-retinal. In particular, no Asp-85 to 14-C-retinal peak was observed.

which again corresponds to the transfer of polarizations between the [14-^{13}C]retinal and [4-^{13}C]Asp-212 positions in both bR_{568} and M_{412}. In similar dark-adapted spectra, no cross-peaks were observed in the bR_{555} state, and again as in the RFDR spectra no cross-peaks were detectable between the retinal and other aspartic acid residues. Spin diffusion spectra recorded with short mixing times (i.e., $\tau_m < 200$ ms) yielded no cross-peaks in all cases.

As estimated from the 2D spin diffusion spectra taken with 2000 ms mixing period, the measured rates of spin diffusion in bR_{568} and M_{412} were $\Gamma = 0.85 \pm 0.30$ kHz and $\Gamma = 0.35 \pm 0.08$ kHz, respectively, at $\omega_r/2\pi = 4.8$ kHz. With the crude assumption that $f(\tau_c)$ in eq 4 is the same as in the glycylglycyl·HCl model compound, the [14-^{13}C]retinal to [4-^{13}C]Asp-212 distances are estimated as 4.5 ± 0.3 and 5.2 ± 0.5 Å in LA and M, respectively, which is in reasonable agreement with the more rigorously quantifiable results from RFDR measurements.

In addition, with the highly reasonable assumption that the proton function $f(\tau_c)$ is virtually the same in the bR_{568} and M_{412} states acquired under identical conditions, the spin diffusion rates provide quantitative information about the *relative* internuclear distances in the two states. Accordingly, these experiments indicate that the internuclear separation from the [14-^{13}C]retinal to [4-^{13}C]Asp-212 increases by $16 \pm 10\%$ in going from bR_{568} to M_{412}. This observation agrees reasonably well with the RFDR results, which indicate an increase of 10%. Because of signal-to-noise limitations, the error bars on the RFDR distances exceed the difference between the measured distances in the two states, and accordingly, the spin diffusion data establishes more unambiguously that the distance increases moderately upon deprotonation of the Schiff base. A conservative estimate for the threshold to observe a cross-peak is 6.0 Å, considering the magnitudes of the observed cross-peaks involving Asp-212. Accordingly, the lack of observable cross-peaks in both the RFDR and spin diffusion spectra indicates that the [14-^{13}C]retinal to [4-^{13}C]Asp-85 distance is greater than 6.0 Å.

DISCUSSION

Solid-state NMR studies have established that in the light-adapted state of bR, the protonated Schiff base is stabilized by a diffuse counterion, presumably involving a H-bonded complex of water with the positively charged Arg-82 side chain and the deprotonated side chains of Asp-212 and Asp-85 (*34*). Although other experimental studies have implied a role for trapped water molecules in this region (*35*), it has only become clear from recent diffraction structures of increasingly high resolution that bound water is intimately associated with the Schiff base and aspartate residues. One water molecule forms H-bonds primarily with the Schiff base and Asp-85 (*11*). The side chain of Asp-212, which interacts with Tyr-57 and Tyr-185, is more weakly associated with the water molecule, and its distance to the retinal chromophore is essentially unaffected by the presence of the water. In the structure of Luecke et al. (*11*), a second water lying further toward the extracellular side is also hydrogen bonded to Asp-85, and a third one links Arg-82 and Glu-204.

Figure 8 illustrates the distances among the ^{13}C-labeled positions that can give rise to potential cross-peaks in the 2D NMR spectra. On the basis of the RFDR experiments, our distance constraints from the 14-^{13}C of the retinal to the 4-^{13}C of Asp-212 and Asp-85 are 4.4 ± 0.6 Å and >6.0 Å, respectively, in the light-adapted state, bR_{568}. As illustrated in Table 2, this measurement is in reasonable agreement with the experimental structures of Pebay-Peyroula et al. (*15*) and Luecke et al. (*11*) and the molecular dynamics simulations of Scharnagl et al. (*6*, *7*), in which a single water molecule is contained among these residues.

While our constraints agree with the experimental results of Pebay-Peyroula et al. (*15*) and Luecke et al. (*11*), they are incompatible with the recent results of Kimura et al. (*13*)

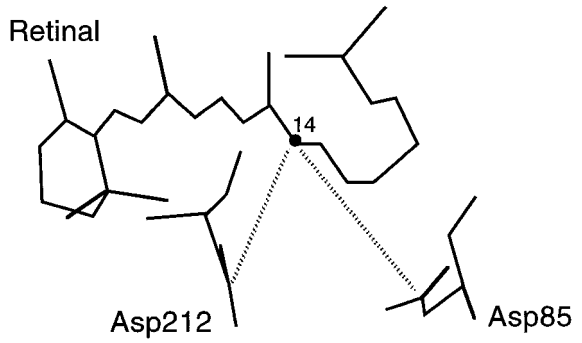

FIGURE 8: Illustration of the retinal, its Schiff base linkage to Lys-216, and the approximate positions of the Asp-85 and Asp-212 residues, whose dipole−dipole couplings are the focus of this work.

Table 2: Geometric Constraints on Aspartates and the Retinal Schiff Base (RSB) Given by Some Recent Experimental and Theoretical Structures

distance (Å)	Grigorieff bR_{568}	Luecke bR_{568}	Scharnagl bR_{568}	Scharnagl M_2
4-Asp-212 to 14-C-retinal	4.29	4.40	4.19	4.94
4-Asp-85 to 14-C-retinal	5.13	<6.0	6.22	7.86
4-Asp-212 to RSB nitrogen	4.13	3.99	4.20	4.29
4-Asp-85 to RSB nitrogen	4.03	4.66	5.39	6.83
4-Asp-212 to 4-Asp-85	5.40	6.51	5.92	5.65

and Grigorieff et al. (*14*), which both predict Asp-85 to [14-C]retinal distances of <5.5 Å. In these latter two structures, the underestimate in the distance accompanies the absence of the crucial water molecule in the models. The shorter NMR distance constraint of 4.4 ± 0.6 Å on the Asp-212 to 14-C-retinal position is essentially consistent with all of these recent experimental structures. In all cases, the Asp-212 side chain is held in position by interactions with the side chains of Tyr-57 and Tyr-185, with a distance to the 14-C-retinal of <4.8 Å (and mostly <4.3 Å).

Although our results agree with the calculations of Scharnagl et al. (*7*), they conflict with the molecular dynamics simulations of Schulten et al. (*9*), which predict distances of >7.5 Å from [14-^{13}C]retinal to [4-^{13}C] in both Asp-85 and Asp-212 based on the placement of several waters in the region encompassed by Asp-212, Asp-85, and the Schiff base. In these calculations, the Schiff base is hydrogen bonded to Asp-85 via two waters and to Asp-212 via a single water. Although molecular dynamics can provide relaxed structures for a given number of waters, it is difficult to predict a priori how many need to be included (*9*, *36*). The NMR measurements presented here provide further evidence for a single water which primarily links Asp-85 and the retinal Schiff base.

The lifetime of the M state of bR is milliseconds in the native photocycle and M is the only deprotonated intermediate (*1*). However, it is otherwise quite complex and has indeed been found to involve several events between deprotonation in the L → M transition and reprotonation in M → N. The key early event is the transfer of the proton from the Schiff base to the Asp-85 side chain. This step drives the ejection of a proton from the extracellular side of the channel with deprotonation of Glu-204 (*3*, *10*). Eventually, a pre-N state, M_N , is formed. This transition is thought to be accompanied by an outward tilt of the F helix, permitting water molecules to enter the relatively hydrophobic channel on the intracellular side (*3*, *35*). Density changes that are consistent with this tilt have been observed in diffraction experiments (*37*).

In most previous NMR studies of the M intermediate of wild-type bR, the conditions under which M is trapped are primarily consistent with an early M state. In these situations, the greater part of the protein conformational change involving the F helix has most likely not yet occurred (*26*, *29*, *30*). It is this state that has been examined in this study. Although this early M state exhibits a 1.7 ppm splitting in the [14-^{13}C]retinal chemical shift, it is thought to represent an equilibrium between two highly similar local conformations. Indeed, similar splittings have not been observed at other ^{13}C-labeled retinal sites, [ϵ-^{13}C]Lys-216, or in ^{15}N spectra of the Schiff base in this state (*26*, *30*). Recently, a strategy to trap a photointermediate state, that may be similar to the late M state, was described (*30*). In the future, it would be interesting to perform similar dipolar recoupling experiments on this state and additional photointermediates, such as L and N, for which cryo-trapping techniques have also been developed for wild-type samples (*28*, *39*).

For the early M state, the NMR measurements reported here place constraints of 4.8 ± 1.0 and >6 Å on the distances of [14-^{13}C]retinal to the [4-^{13}C] in Asp-212 and Asp-85, respectively. The RFDR analysis for Asp-212 is consistent with the distance increase of 0.7 Å from bR_{568} to the $M_{2(O)}$ and $M_{2(-)}$ states calculated by the molecular dynamics simulations of Scharnagl et al. (*6*, *7*). Likewise, the spin diffusion experiments predict a 16 ± 10% increase in the distance, consistent with the 17% increase given by the simulations. In brief, the predictions of Scharnagl et al. (*6*, *7*) are that initial transfer of the proton from the Schiff base to Asp-85 [resulting in the short-lived $M_{1(0)}$] is followed by a downward tilt of Arg-82 [resulting in $M_{2(0)}$] and a pH sensitive extracellular release of a proton from Glu-204 [resulting in $M_{2(-)}$]. In the calculations, the geometric relationships between Asp-85, Asp-212, and the retinal chromophore are virtually identical in the $M_{2(0)}$ and $M_{2(-)}$ states. Previous NMR results have found evidence of a perturbation of Arg-82 and the present results support the predicted geometry between the retinal and Asp-212.

Clearly, the water molecules in the binding pocket play an important role in proton transport (*7*, *8*). Further, the position and number of water molecules are important factors in defining the structure of the retinal-binding pocket near the Schiff base during each stage of the photocycle. It is clear from recent diffraction studies (*11*), theoretical calculations (*7*), and the structural data from the NMR experiments presented here that a single water separates Asp-85 from the retinal Schiff base linkage in both bR_{568} and M. The observable cross-peak between [4-^{13}C]Asp-212 and [14-^{13}C]-retinal indicates that this water molecule does not lie between these sites. The small increase in distance upon M formation is consistent with a slight upward shift in the retinal near the Schiff base and a relatively fixed Asp-212 side chain. Possibly the stable side-chain arrangement of Asp-212 is quite important to the reprotonation step, as well as to the stability of the binding pocket. Interestingly, mutagenesis of Asp-212 to glutamic acid reduces proton-pumping efficiency even more than similar substitutions of either Asp-96 or Asp-85 (*2*).

CONCLUSIONS

The NMR structural data presented here are consistent with recent experimental structures of the resting state of bR (*11*, *15*). They also provide experimental evidence that supports theoretical models of the formation of the deprotonated Schiff base M_{412} intermediate of the photocycle (*7*).

NMR distance measurements based on dipole−dipole couplings among ^{13}C labels reveal that the distance from the carboxyl carbon of Asp-212 to the [14-C]retinal site of bR is 4.4 ± 0.6 Å in bR_{568}, 4.8 ± 1.0 Å in early M_{412}, and >6.0 Å in bR_{555}. The carboxyl carbons of Asp-85, Asp-96, and Asp-115 are >6.0 Å from the [14-C]retinal site in all three states of bR. Further, no cross-peaks are observed from [14-^{13}C]retinal in bR_{555} to any Asp residue. For bR_{568}, these results underscore that the water molecule, interposed within the quadrupolar structure formed by the Schiff base, Asp-85, Asp-212, and Arg-82, primarily serves to separate the Schiff base from Asp-85, although Asp-85 is the proton acceptor. The NMR data also suggest that similar relationships persist in the early M_{412} state.

NMR experiments based on both multiple pulse and spin diffusion experiments have yielded consistent results for aspartate−retinal distance constraints, providing data complimentary to previous experimental and theoretical results. These measurements together with previous studies of retinal-Schiff base conformations using RFDR (*23*) and other recoupling methods (*29*, *41*) illustrate the enhanced utility of current solid-state NMR methods. These techniques exploit not only chemical shifts and orientational information (*42*), but also the distance information contained in dipole−dipole couplings.

ACKNOWLEDGMENT

The authors thank Dr. Susan Pochapsky for assistance with 2D data processing, and R. Henderson, K. Schulten, C. Scharnagl, J. Lanyi, Y. Kimura, and their respective research groups for providing their bR coordinates.

NOTE ADDED IN PROOF:

Since this paper was submitted and accepted, three new crystal structures of bR have been reported [Essen, L.-O., Siegert, R., Lehmann, W. D., and Osterhelt, D. (1998) *Proc. Natl. Acad. Sci. U.S.A. 95*, 11673−11678; Luecke, H., Schobert, B., Richter, H.-T., Cartailler, J. P., Lanyi, J. K. (1999) *J. Mol. Biol. 291*, 899−911; Luecke, H., Schobert, B., Richter, H.-T., Cartailler, J. P., Lanyi, J. K. (1999) *Science 286*, 255−260]. Of particular relevance for this manuscript is the report by Luecke et al. (1999) of the structure of the D96N bR in the resting state and the M_N state. In the latter, the Asp-212−Ret-14C distance is reported to be 5.79 Å, which is longer than we measure for early M (4.8 ± 1.0 Å). The X-ray distance would result in an extremely weak cross peak in the dipolar recoupling experiment. Our contrasting result maybe due to some combination of (a) differences between early M and late M, (b) the differences between the wild-type and D96N mutant protein or, (c) the targets used in modeling the crystallographic electron density.

REFERENCES

1. Ebrey, T. (1993) in *Thermodynamics of Membrane Receptors and Channels* (Jackson, M. B., Ed.) pp 353−387, CRC Press, Boca Raton.
2. Khorana, H. G. (1993) *Proc. Natl. Acad. Sci. U.S.A. 90*, 1166−1171.
3. Lanyi, J. K. (1997) *J. Biol. Chem. 272*, 31209−31212.
4. Henderson, R., Baldwin, J. M., Ceska, T. A., Zemlin, F., Beckmann, E., and Downing, K. H. (1990) *J. Mol. Bio. 213*, 899−929.
5. Sampogna, R. V., and Honig, B. (1994) *Biophys. J. 66*, 1341−1352.
6. Scharnagl, C., Hettenkofer, J., and Fischer, S. F. (1994) *Int. J. Quantum Chem.: Quantum Biol. Symp. 21*, 33−56.
7. Scharnagl, C., Hettenkofer, J., and Fischer, S. F. (1995) *J. Phys. Chem. 99*, 7787−7800.
8. Xu, D., Sheves, M., and Schulten, K. (1995) *Biophys. J. 69*, 2745−2760.
9. Schulten, K., Humphrey, W., Logunox, I., Sheves, M., and Xu, D. (1995) *Isr. J. Chem. 35*, 447−464.
10. Lanyi, J. K. (1998) *Biochim. Biophys. Acta 1365*, 17−22.
11. Luecke, H., Richter, H.-T., and Lanyi, J. K. (1998) *Science 280*, 1934−1937.
12. Braiman, M. S., Mogi, T., Marti, T., Stern, L. J., Khorana, G. H., and Rothschild, K. J. (1988) *Biochem. 27*, 8516.
13. Kimura, Y., Vassylyev, D. G., Miyazawa, A., Kidera, A., Matsushima, M., Misuoka, K., Muata, K., Hirai, T., and Fujiyoshi, Y. (1997) *Nature 389*, 206−211.
14. Grigorieff, N., Ceska, T. A., Downing, K. H., Baldwin, J. M., and Henderson, R. (1996) *J. Mol. Biol. 259*, 393−421.
15. Pebay-Peyroula, E., Rummel, G., Rosenbusch, J. P., and Landau, E. M. (1997) *Science 277*, 1676.
16. Metz, G., Siebert, F., and Engelhard, M. (1992) *FEBS Lett. 303*, 237−241.
17. Bennett, A. E., Ok, J. H., Griffin, R. G., and Vega, S. (1992) *J. Chem. Phys. 96*, 8624−8627.
18. Bennett, A. E., Rienstra, C. M., Griffiths, J. M., Zhen, W., and Lansbury, P. T., Jr. (1998) *J. Chem. Phys. 108*, 9463−9479.
19. Vanderhart, D. L. (1987) *J. Magn. Reson. 72*, 13.
20. Tycko, R., and Dabbagh, G. (1992) *Isr. J. Chem. 32*, 179−184.
21. Suter, D., and Ernst, R. R. (1985) *Phys. Rev. B 32*, 5608.
22. Kubo, A., and McDowell, C. A. (1988) *J. Chem. Soc., Faraday Trans. 84*, 3713.
23. Griffiths, J. M., Lakshmi, K. V., Bennett, A. E., Raap, J., van der Wielen, C. M., Lugtenburg, J., Herzfeld, J., and Griffin, R. G. (1994) *J. Am. Chem. Soc. 116*, 10178−10181.
24. Metz, G., Siebert, F., and Engelhard, M. (1992) *Biochemistry 31*, 455−462.
25. Engelhard, M., Hess, B., Emeis, D., Metz, G., Kreutz, W., and Siebert, F. (1989) *Biochemistry 28*, 3967.
26. Farrar, M. R., Lakshmi, K. V., Smith, S. O., Brown, R. S., Raap, J., Lugtenburg, J., Griffin, R. G., and Herzfeld, J. (1993) *Biophys. J. 65*, 310−315.
27. Gullion, T., Baker, D. B., and Conradi, M. S. (1990) *J. Magn. Res. 89*, 479.
28. Hu, J. G., Sun, B. Q., Petkova, A. T., Griffin, R. G., and Herzfeld, J. (1997) *Biochemistry 36*, 9316−9322.
29. Lakshmi, K. V., Auger, M., Raap, J., Lugtenburg, J., Griffin, R. G., and Herzfeld, J. (1993) *J. Am. Chem. Soc. 115*, 8515−8516.
30. Hu, J. G., Sun, B. Q., Bizounok, M., Hatcher, M. E., Lansing, J. C., Raap, J., Verdegem, P. J. E., Lugtenburg, J., Griffin, R. G., and Herzfeld, J. (1998) *Biochemistry 37*, 8088−8096.
31. Smith, S. O., de Groot, H. J. M., Gebhard, R., Courtin, J. M. L., Lugtenburg, J., Herzfeld, J., and Griffin, R. G. (1989) *Biochemistry 28*, 8897.
32. Bennett, A. E. (1995) Massachusetts Institute of Technology.
33. VanderHart, D. L., Earl, W. L., and Garroway, A. N. (1981) *J. Magn. Reson. 44*, 361.
34. deGroot, H. J. M., Harbison, G. S., Herzfeld, J., and Griffin, R. G. (1989) *Biochemistry 28*, 3346−3353.
35. Maeda, A., Kandori, H., Yamazaki, Y., Nishimura, S., Hatanaka, M., Chon, Y.-S., Sasaki, J., Needleman, R., and Lanyi, J. K. (1997) *J. Biochem. 121*, 399−406.

36. Humphrey, W., Logunov, I., Schulten, K., and Sheves, M. (1994) *Biochemistry 33*, 3668−3678.
37. Subramaniam, S., Gerstein, M., Oesterhelt, D., and Henderson, R. (1993) *EMBO J. 12*, 1−8.
38. Honig, B., Ottolenghi, M., and Sheves, M. (1995) *Isr. J. Chem. 35*, 429−446.
39. Lakshmi, K. V., Farrar, M. R., Raap, J., Lugtenburg, J., Griffin, R. G., and Herzfeld, J. (1994) *Biochemistry 33*, 8853−8857.
40. Ulrich, A. S., Wallat, I., Heyn, M. P., and Watts, A. (1995) *Nat. Struct. Biol. 2*, 190−192.
41. Thompson, L. K., McDermott, A. E., Raap, J., van der Wielen, C. M., Lugtenburg, J., Herzfeld, J., and Griffin, R. G. (1992) *Biochemistry 31*, 7931−7938.
42. Engelhard, M., and Bechinger, B. (1995) *Isr. J. Chem. 35*, 273−288.

BI991106D